

Geometric structure of N_2O^{q+} (q=5, 6) studied by Ne^{8+} ion-induced Coulomb explosion imaging

Xi Zhao(赵曦), Xu Shan(单旭), Xiaolong Zhu(朱小龙), Lei Chen(陈磊), Zhenjie Shen(沈镇捷), Wentian Feng(冯文天), Dalong Guo(郭大龙), Dongmei Zhao(赵冬梅), Ruitian Zhang(张瑞田), Yong Gao(高永), Zhongkui Huang(黄忠魁), Shaofeng Zhang(张少锋), Xinwen Ma(马新文), and Xiangjun Chen (陈向军)

Citation: Chin. Phys. B, 2021, 30 (**11**): 113302. DOI: 10.1088/1674-1056/abff45
Journal homepage: http://cpb.iphy.ac.cn; http://iopscience.iop.org/cpb

What follows is a list of articles you may be interested in

Direct Coulomb explosion of N_2O^{2+} induced by monochromatic extreme ultraviolet photons at 38.5 eV

Min Zhang(张敏), B Najjari, Bang Hai(海帮), Dong-Mei Zhao(赵冬梅), Jian-Ting Lei(雷建廷), Da-Pu Dong(董达谱), Shao-Feng Zhang(张少锋), Xin-Wen Ma(马新文)
Chin. Phys. B, 2020, 29 (**6**): 063302. DOI: 10.1088/1674-1056/ab8629

Theoretical investigations of collision dynamics of cytosine by low-energy (150-1000 eV) proton impact

Zhi-Ping Wang(王志萍), Feng-Shou Zhang(张丰收), Xue-Fen Xu(许雪芬), Chao-Yi Qian(钱超义)
Chin. Phys. B, 2020, 29 (**2**): 023401. DOI: 10.1088/1674-1056/ab6313

Interaction of H_2^+ molecular beam with thin layer graphene foils

Min Li(李敏), Guo-Feng Qu(曲国峰), Yi-Zhou Wang(王亦舟), Zhou-Sen Zhu(朱洲森), Mian-Gong Shi(师勉恭), Mao-Lei Zhou(周茂蕾), Dong Liu(刘东), Zi-Xu Xu(徐子虚), Ming-Jiang Song(宋明江), Jun Zhang(张俊), Fan Bai(白帆), Xiao-Dong Liao(廖小东), Ji-Feng Han(韩纪锋)
Chin. Phys. B, 2019, 28 (**9**): 093401. DOI: 10.1088/1674-1056/ab33f2

Coulomb explosion of CS_2 molecule under an intense femtosecond laser field

Xiao Wang(王潇), Jian Zhang(张健), Shi-An Zhang(张诗按), Zhen-Rong Sun(孙真荣)
Chin. Phys. B, 2016, 25 (**5**): 053301. DOI: 10.1088/1674-1056/25/5/053301

Compton profile of molecular hydrogen

Zhao Xiao-Li, Yang Ke, Xu Long-Quan, Ma Yong-Peng, Yan Shuai, Ni Dong-Dong, Kang Xu, Liu Ya-Wei, Zhu Lin-Fan
Chin. Phys. B, 2015, 24 (**3**): 033301. DOI: 10.1088/1674-1056/24/3/033301

Geometric structure of N_2O^{q+} ($q = 5, 6$) studied by Ne^{8+} ion-induced Coulomb explosion imaging*

Xi Zhao(赵曦)[1], Xu Shan(单旭)[1,†], Xiaolong Zhu(朱小龙)[2], Lei Chen(陈磊)[1], Zhenjie Shen(沈镇捷)[1], Wentian Feng(冯文天)[2], Dalong Guo(郭大龙)[2], Dongmei Zhao(赵冬梅)[2], Ruitian Zhang(张瑞田)[2], Yong Gao(高永)[2], Zhongkui Huang(黄忠魁)[2], Shaofeng Zhang(张少锋)[2], Xinwen Ma(马新文)[2,‡], and Xiangjun Chen (陈向军)[1]

[1] *Hefei National Laboratory for Physical Sciences at the Microscale and Department of Modern Physics, University of Science and Technology of China, Hefei* 230026, *China*

[2] *Institute of Modern Physics, Chinese Academy of Sciences, Lanzhou* 730000, *China*

(Received 31 March 2021; revised manuscript received 30 April 2021; accepted manuscript online 10 May 2021)

We report the study on the complete three-body Coulomb explosion (CE) of N_2O^{q+} ($q = 5, 6$) induced by 56-keV/u Ne^{8+} ion collision with N_2O gaseous molecule. Six CE channels for N_2O^{5+} and seven for N_2O^{6+} are identified by measuring three ionic fragments and the charge-changed projectile in quadruple coincidence. Correspondingly the kinetic energy release (KER) and momentum correlation angle (MCA) distributions of three ionic fragments for each of the CE channels are also deduced. Numerical computation is presented to reconstruct the geometric structure of N_2O^{q+} prior to dissociation based on the measured KER and MCA. The N–N and N–O bond lengths and the N–N–O bond angles of N_2O^{q+} for each of the channels are determined.

Keywords: Coulomb explosion, kinetic energy release, molecular geometry, ion collision, nitrous oxide (N_2O)

PACS: 34.50.Gb, 34.80.Ht **DOI:** 10.1088/1674-1056/abff45

1. Introduction

The geometry or configuration of a molecule is a central issue in molecular physics, which governs the molecular structure and properties. It is well known that electron diffraction, microwave, and infrared spectroscopy methods are widely used to determine molecular structures. Coulomb explosion imaging (CEI) technique[1,2] is an alternative to spectroscopy for yielding molecular geometric information. The basic principle of CEI consists of quick ionizations of a molecule induced by thin foils, photons, electrons, or ions, and thereby creating a multiply charged molecular ion which undergoes a fast dissociation due to the Coulomb repulsion between fragment cations. By measuring the final vector momenta of the ionic fragments in coincidence, one can reconstruct the initial positions of the fragments and thus obtain an image of the molecule. Development of the recoil momentum spectroscopy or reaction microscope[3,4] promoted the application of CEI to imaging the structures of diatomic or polyatomic molecules and van der Waals complexes.[5–25] For lowly charged molecular ions, due to the existence of predissociative or metastable states, Coulomb explosion occurs also through these non-Coulombic states. As a result, the critical nuclear distance R_c of molecular ions at the moment of explosion reconstructed by using the Coulomb potential model was found to overestimate the equilibrium separation R_e of the neutral molecule.[6] In order to derive the accurate structural parameters by CEI, highly charged molecular ions were paid more attention. Intense laser fields can conveniently make more electrons of a molecule be ionized and thereby form a highly charged molecular ion that readily undergoes Coulomb explosion (CE). However, intense laser pulses also could result in the deformation of molecular structures during the multiple ionization process.[5–12] The R_c determined by intense laser CEI experiments was found to be approximately two to three times R_e. When the laser pulse duration is shorter than 10 fs, that is, the ionization interaction of laser with a molecule is fast so that the molecular geometry still remains, the reconstructed R_c could represent R_e.[5–7,11–13] Electron impact experiment also can create highly charged molecular ions and obtain accurate structural parameters such as bond lengths and angles by using the CEI technique,[15,16] although it presents relatively small multi-ionization cross-sections. Collision of highly charged ion (HCI) with molecules is another way to well produce high charge molecular ions through electron capture and transfer ionization processes. But researches on imaging molecular geometry by the HCI induced CEI method are relatively scarce.[17–19]

In the present study, we apply the CEI technique to the

*Project supported by the National Key Research and Development Program of China (Grant Nos. 2017YFA0402300 and 2017YFA0303501) and the Strategic Priority Research Program of Chinese Academy of Sciences (Grant No. XDB34000000). The authors thank the staff of the 320-kV platform for multidisciplinary research with highly charged ions at the Institute of Modern Physics, Chinese Academy of Sciences, for their technical support.

†Corresponding author. E-mail: xshan@ustc.edu.cn

‡Corresponding author. E-mail: x.ma@impcas.ac.cn

© 2021 Chinese Physical Society and IOP Publishing Ltd

Coulomb explosion of nitrous oxide (N_2O) induced by the HCI collision. N_2O is the prototype of asymmetric triatomic molecules including two different N–N and N–O bonds. The study of imaging N_2O geometry may bring a suggestion to the polyatomic molecules which are confronted with great challenges to quantitatively determine the geometric parameters. The CE dynamics of N_2O^{q+} ($q \geq 2$) induced by electron, ion, and photon collisions have been extensively studied experimentally and theoretically.[8–10,26–43] Most of the previous works concentrated on the two-body fragmentation of N_2O^{q+} ($q = 2, 3$). Relatively few works[8–10,29–31] presented the complete three-body CE process of highly charged N_2O^{q+} ($q \geq 3$). In the HCI collision experiments of Werner *et al.*[29] and Khan *et al.*,[30] the kinetic energy release (KER) distributions for a part of three-body CE channels of N_2O^{q+} (q = 3–7) have been obtained and explained using the simple CE model in which the fragment ions are treated as point charges at the equilibrium bond lengths. As for the geometry of N_2O^{q+}, only the laser-induced CE experiments have been performed to tentatively derive the structural parameters by Hishikawa *et al.*[8] and Ueyama *et al.*[9] But the obtained R_c of N_2O^{q+} was found to be about 1.4–2 times larger than the R_e of neutral N_2O. In addition, the coexistence of sequential and non-sequential three-body dissociation processes of N_2O^{3+} and N_2O^{4+} has been revealed,[10] which are no longer pure concerted Coulomb explosions.

Here, we focus on the concerted three-body CE channels of highly charged N_2O^{5+} and N_2O^{6+} induced by 56 keV/u Ne^{8+} ion collisions. Six CE channels for N_2O^{5+} and seven for N_2O^{6+} are identified by measuring three ionic fragments and the charge-changed projectile in quadruple coincidence. Utilizing the experimental KER and momentum correlation angles (MCA) of the three ionic fragments for each of the CE channels, the N–N and N–O bond lengths and N–N–O bond angles of N_2O^{q+} prior to dissociation are deduced by numerical computation.

2. Experimental method

The present experiment is performed by using the reaction microscope on the 320-kV platform for multidisciplinary research with highly charged ions at the Institute of Modern Physics in Lanzhou. The detailed description of the experimental setup has been presented previously.[44,45] Here only a brief introduction is given. The Ne^{8+} ions are produced in the electron cyclotron resonance ion source and accelerated to the experimental energy of 56 keV/u for collisions. After being collimated by two sets of adjustable slits and purified by several sets of electrostatic deflectors, the ion beam is transported to the target chamber and intersected with a cold supersonic N_2O gas jet which is introduced into the reaction chamber through a nozzle of 0.03 mm diameter and picked up by two skimmers of 0.05 mm diameter. A Wiley–McLaren type time of flight (TOF) system[46] is employed to extract and transfer the ionic products of N_2O into a time- and position-sensitive detector (PSD-R). The primary beam of Ne^{8+} projectile is collected by a Faraday cup, and the charge-changed projectile is analyzed by a pair of electrostatic deflectors downstream of the collision zone combined with another position-sensitive detector (PSD-P). All position-sensitive detectors are constructed as a combination of the microchannel plate with the standard delay line anode. The signal and data acquisition system is triggered by the signal from the PSD-P, and the fragment ions are recorded in coincidence with the scattered projectile. The information on the position and TOF of the ionic fragments is recorded event by event. In the off-line data analysis, the three-dimensional momentum vector for each of the fragment ions can be obtained by the measured TOF and position (x, y) on the PSD-R. Through the correlation analysis on the TOFs and the momentum conservation of three fragment ions, the complete three-body CE channels can be determined, i.e., $N_2O^{q+} \rightarrow N^{l+} + N^{m+} + O^{n+}$ ($q = l + m + n$). For the convenience of discussion, the specific channels are denoted as (lmn) in the following parts.

3. Results and discussion

Various fragmentation channels of N_2O^{q+} are opened in the present experiment. Here we only concentrate on the concerted three-body CE channels of the highly charged N_2O^{5+} and N_2O^{6+}. It is well established that for a linear triatomic N_2O^{q+}, the fragment ion from the central nitrogen atom (hereafter as N_c), relative to the terminal nitrogen (hereafter as N_t) and oxygen atoms, is usually assigned the smallest momentum (kinetic energy) in the concerted three-body CE process. So the two nitrogen ions with the same charge from N_2O^{q+} breakup can be distinguished unambiguously. In this case by further utilizing the TOF correlation analysis and the momentum conservation of the three fragment ions, six CE channels for N_2O^{5+} and seven for N_2O^{6+} are identified as follows:

$$
\begin{aligned}
&N_2O^{5+} \rightarrow N_t^+ + N_c^+ + O^{3+} \quad (113),\\
&N_2O^{5+} \rightarrow N_t^+ + N_c^{2+} + O^{2+} \quad (122),\\
&N_2O^{5+} \rightarrow N_t^{2+} + N_c^+ + O^{2+} \quad (212),\\
&N_2O^{5+} \rightarrow N_t^+ + N_c^{3+} + O^+ \quad (131),\\
&N_2O^{5+} \rightarrow N_t^{3+} + N_c^+ + O^+ \quad (311),\\
&N_2O^{5+} \rightarrow N_t^{2+} + N_c^{2+} + O^+ \quad (221),\\
&N_2O^{6+} \rightarrow N_t^+ + N_c^{2+} + O^{3+} \quad (123),\\
&N_2O^{6+} \rightarrow N_t^{2+} + N_c^+ + O^{3+} \quad (213),\\
&N_2O^{6+} \rightarrow N_t^+ + N_c^{3+} + O^{2+} \quad (132),\\
&N_2O^{6+} \rightarrow N_t^{3+} + N_c^+ + O^{2+} \quad (312),\\
&N_2O^{6+} \rightarrow N_t^{2+} + N_c^{2+} + O^{2+} \quad (222),\\
&N_2O^{6+} \rightarrow N_t^{2+} + N_c^{3+} + O^+ \quad (231)\\
&N_2O^{6+} \rightarrow N_t^{3+} + N_c^{2+} + O^+ \quad (321).
\end{aligned}
$$

In order to depict the fragmentation mechanism for each of these channels, the measured momenta of the three atomic

ions from N_2O^{5+} and N_2O^{6+} breakup are displayed by using Newton diagrams in Figs. 1(a1)–1(f1) and 2(a1)–2(g1), respectively. In the Newton diagrams, the momentum vector of the oxygen ion O^{n+} is represented by a horizontal arrow fixed at one arbitrary unit. The momentum vectors of two nitrogen ions N_t^{l+} and N_c^{m+} are mapped in the left of the plot, in which their momentum magnitudes are normalized to that of the oxygen ion. One can see that the island of N_c^{m+} for each of the thirteen channels is located near the origin of the Newton diagrams indicating that very small momenta are assigned to N_c^{m+} at the moment of emitting. Actually, the terminal N_t^{l+} and O^{n+} have shared almost all the momenta from the Coulomb explosion of N_2O^{q+}. Such momentum correlation characteristics of the three atomic ions in Newton diagrams reveal a completely concerted CE process of the highly charged N_2O^{q+}.

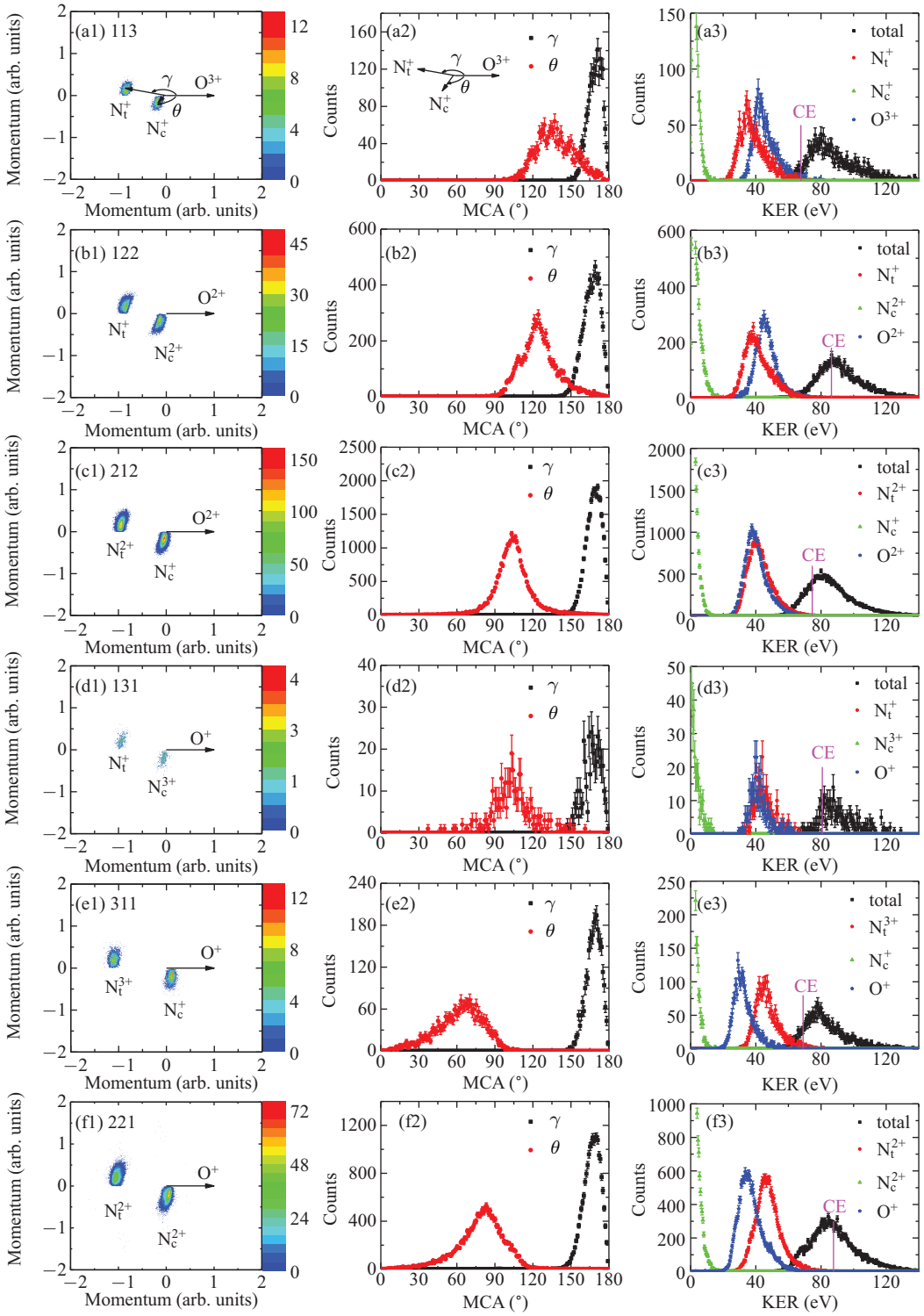


Fig. 1. The experimental Newton diagrams, momentum correlation angle (MCA) and the kinetic energy release (KER) distributions for three atomic ions of the six CE channels of N_2O^{5+}. (a1)–(f1) Newton diagrams. (a2)–(f2) MCA distributions. (a3)–(f3) KER distributions, the vertical lines denote the predictions of the CE model.

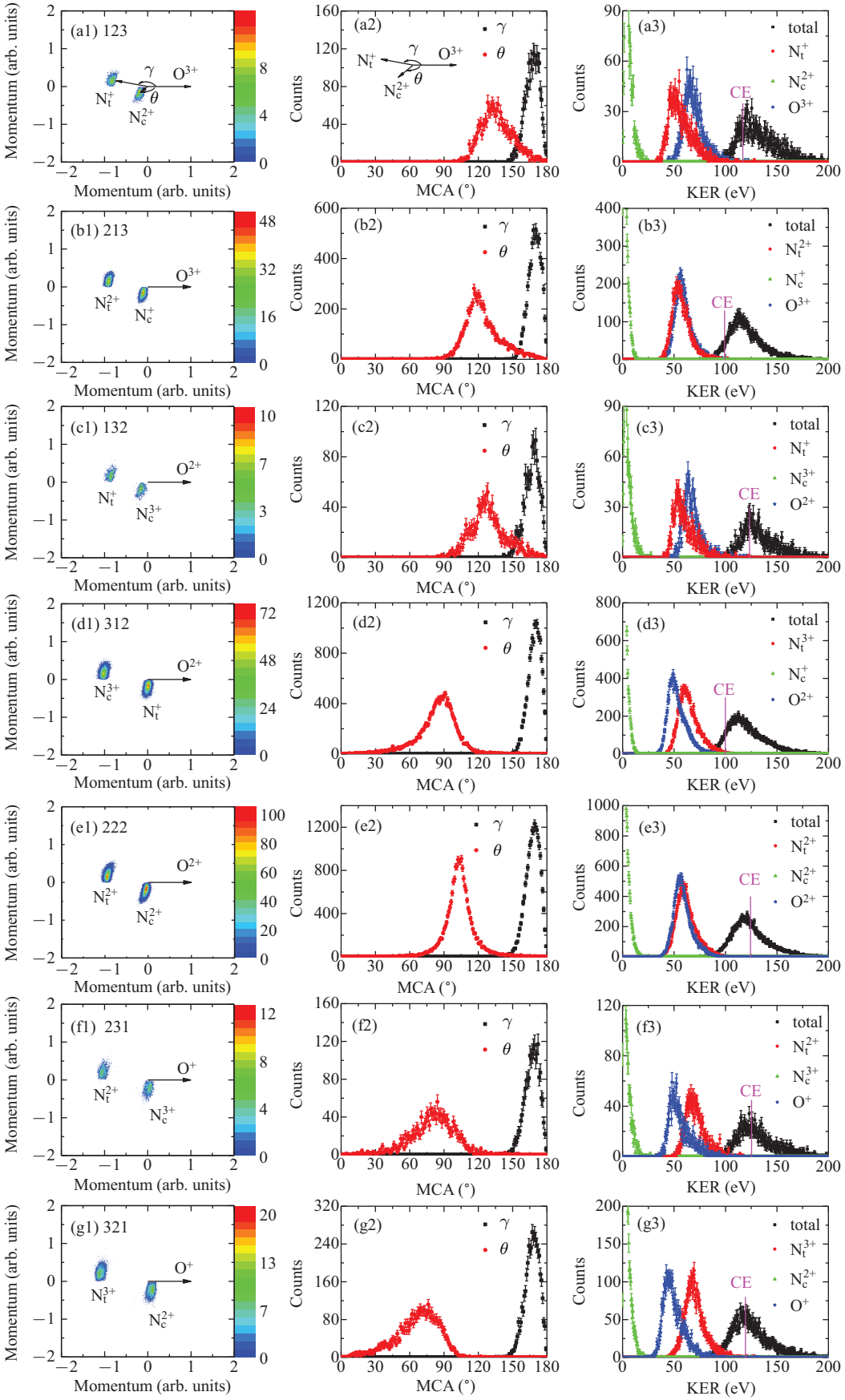


Fig. 2. The same as that of Fig. 1, but for the seven CE channels of N_2O^{6+}.

The islands in Newton diagrams can reflect the geometric distributions of fragments, while the momentum correlation angle (MCA) α can be obtained by the momentum vectors ($\boldsymbol{p}_1$, $\boldsymbol{p}_2$) of two associated ions,

$$\alpha = \cos^{-1}\left(\frac{\boldsymbol{p}_1 \cdot \boldsymbol{p}_2}{|\boldsymbol{p}_1||\boldsymbol{p}_2|}\right). \quad (1)$$

Here we denote the MCA between N_t^{l+} and O^{n+} as γ, and that of N_c^{m+} and O^{n+} as θ. The MCA distributions for the six CE channels of N_2O^{5+} are shown in Figs. 1(a2)–1(f2) and those of N_2O^{6+} in Figs. 2(a2)–2(g2). The distributions of γ angles range from 150° to 180° with the most probable value of about 170°. While the θ angle distributions are very different, showing the remarkable dependence on the channels. A tendency is obvious that the θ angle enlarges with the increase of oxygen ion charges simultaneously. The charge assignment of N_2O^{q+} to three atoms at the moment of fragmentation should be responsible for this case.

The KER distributions for the six CE channels of N_2O^{5+} have been obtained by the measured momenta of the three fragment ions and shown in Figs. 1(a3)–1(f3). Similarly, those of N_2O^{6+} are presented in Figs. 2(a3)–2(g3). For comparison, the theoretical KER values predicted by the CE model are also plotted using the vertical lines in the figures. In the CE model, the fragment ions are regarded as point charges and their distances are assumed to be the R_e of N_2O ($R_{N-N} = 1.13$ Å and $R_{N-O} = 1.19$ Å[47]). In this case, the total KER values of N_2O^{5+} and N_2O^{6+} can be calculated by the following equation:

$$E_{KER} = 14.4 \times \sum_{i>j=1}^{3} \frac{q_i q_j}{r_{ij}}, \quad (2)$$

where q_i and q_j are the charges of the fragment ions, and r_{ij} is their distance. The calculated KER values for the six CE channels of N_2O^{5+} and those of N_2O^{6+} are listed in Table 1, together with the experimental KER peak values, as well as the KER ratio of the CE calculation and the measurement.

Table 1. The total KER and the derived geometric parameters for the CE channels of N_2O^{5+} and N_2O^{6+}.

Channel	KER (eV)			Bond angle (°)	Bond length (Å)	
	CE	Exp.	CE/Exp.		N–N	N–O
(113)	67.7	82.8	0.82	168	0.81 ± 0.01	1.07 ± 0.01
(122)	86.4	89.2	0.97	172	1.02 ± 0.10	1.22 ± 0.07
(212)	74.6	82.7	0.90	168	1.01 ± 0.04	1.10 ± 0.05
(131)	80.8	86.4	0.94	173	1.00 ± 0.07	1.18 ± 0.10
(311)	69.0	79.2	0.87	172	0.95 ± 0.05	1.15 ± 0.13
(221)	87.7	85.6	1.02	173	1.17 ± 0.03	1.25 ± 0.03
(123)	116.8	122.7	0.95	173	1.00 ± 0.10	1.16 ± 0.05
(213)	99.1	116.0	0.85	168	0.95 ± 0.05	1.06 ± 0.06
(132)	123.4	127.5	0.97	173	1.00 ± 0.10	1.22 ± 0.08
(312)	99.8	115.9	0.86	169	0.96 ± 0.04	1.07 ± 0.07
(222)	124.3	120.4	1.03	171	1.16 ± 0.05	1.25 ± 0.05
(231)	125.3	124.8	1.00	174	1.15 ± 0.03	1.23 ± 0.04
(321)	119.4	120.2	0.99	173	1.13 ± 0.03	1.23 ± 0.07

As shown in Figs. 1(a3)–1(f3), for the CE channels (113), (212) and (311) of N_2O^{5+}, the KER values estimated by the CE model largely underestimate the presently measured KER peak values. The specific deviations can be seen in Table 1. But for the channels (122) and (221), the CE predictions can agree well with the most probable values of the experimental KER distributions. Werner *et al.*[29] reported the KER value (∼ 84.0 eV) for the (221) channel of $N_2O^{5+} \rightarrow N_t^{2+} + N_c^{2+} + O^+$ in 5.9 MeV/u Xe^{18+} collision experiment, consistent with the present experiment (85.6 eV) but inconsistent with the previous measurement (75 eV) of Khan *et al.* in 1 MeV Xe^{15+} ion collision.[30] For the seven CE channels of N_2O^{6+}, their KER distributions are presented in Figs. 2(a3)–2(g3). One can see the serious KER deviation of the CE predictions from the measurements for (213) and (312) channels and the good agreements for the channels of (123), (132), (222), (231) and (321). The KER value (∼ 116 eV) of Werner *et al.*[29] for the (222) channel is approximately close to the present measurement (120.4 eV) and the CE prediction (124.3 eV), while that (112 eV) of Khan *et al.*[30] still remained a slightly large deviation. Generally, for the CE channels of N_2O^{5+} and N_2O^{6+}, the experimental KER values from Khan *et al.*[30] are relatively smaller than the present results with the deviation of about 3–12 eV except for the channel (231).

The bond angle and bond lengths of N_2O^{q+} just before explosion can be reconstructed through the measured MCA and KER based on the CE model. Although the MCA γ is directly related to the molecular bond angle, generally there is no analytical relationship between them.[14,15] In order to obtain their relationship, a numerical simulation for the explosion dynamics of N_2O^{5+} and N_2O^{6+} is performed by assuming the fragment ions moving in a Coulomb repulsive potential. In the simulation, the N–N and N–O bond lengths which change synchronously in the same step, as well as the bond angle are regarded as independent variables. The dependences of MCA γ as functions of the N–N–O bond angle and the N–N and N–O bond lengths for the CE channels of N_2O^{5+} and N_2O^{6+} are shown in Figs. 3(a1)–3(f1) and 4(a1)–4(g1), respectively. One can see that the relationships between the MCA γ and the bond angle for all channels are obviously independent of

the bond length variation, very similar to the case of CO_2 molecule.[14,15] Their relationships therefore can be derived at the R_e of N_2O ($R_{N-N} = 1.13$ Å, $R_{N-O} = 1.19$ Å[47]), as shown in Figs. 3(a2)–3(f2) and 4(a2)–4(g2). According to such numerical relationships, the N–N–O bond angle distributions for all channels have been obtained by transforming the measured MCA γ distributions, which are depicted in Figs. 3(a3)–3(f3) and 4(a3)–4(g3), respectively. So the most probable values of the N–N–O bond angle for all channels are determined to be about 170°, as listed in Table 1, indicating that the highly charged N_2O still keeps an approximately linear structure. The deviation from 180° should be ascribed to the molecular vibrations, especially bending vibrations. A similar phenomenon has been found and explained by the vibrational effect in the studies of CO_2 molecule.[14–17]

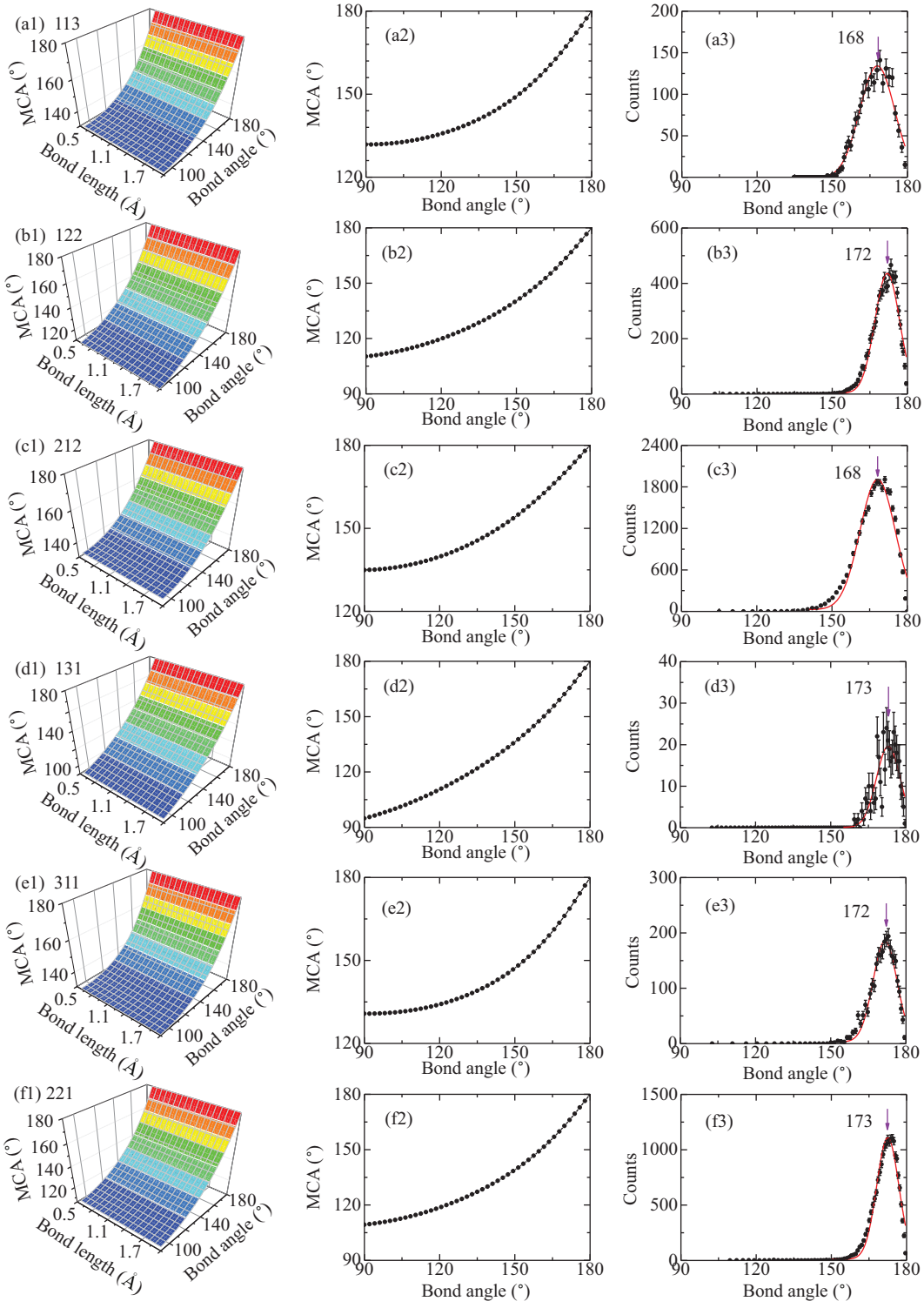


Fig. 3. Simulations and observations for the six CE channels of N_2O^{5+}. (a1)–(f1) The relationship between momentum correlation angle γ, bond lengths and bond angle. (a2)–(f2) The relationship between the momentum correlation angle γ and the bond angle at a fixed bond length. (a3)–(f3) The obtained bond angle distributions.

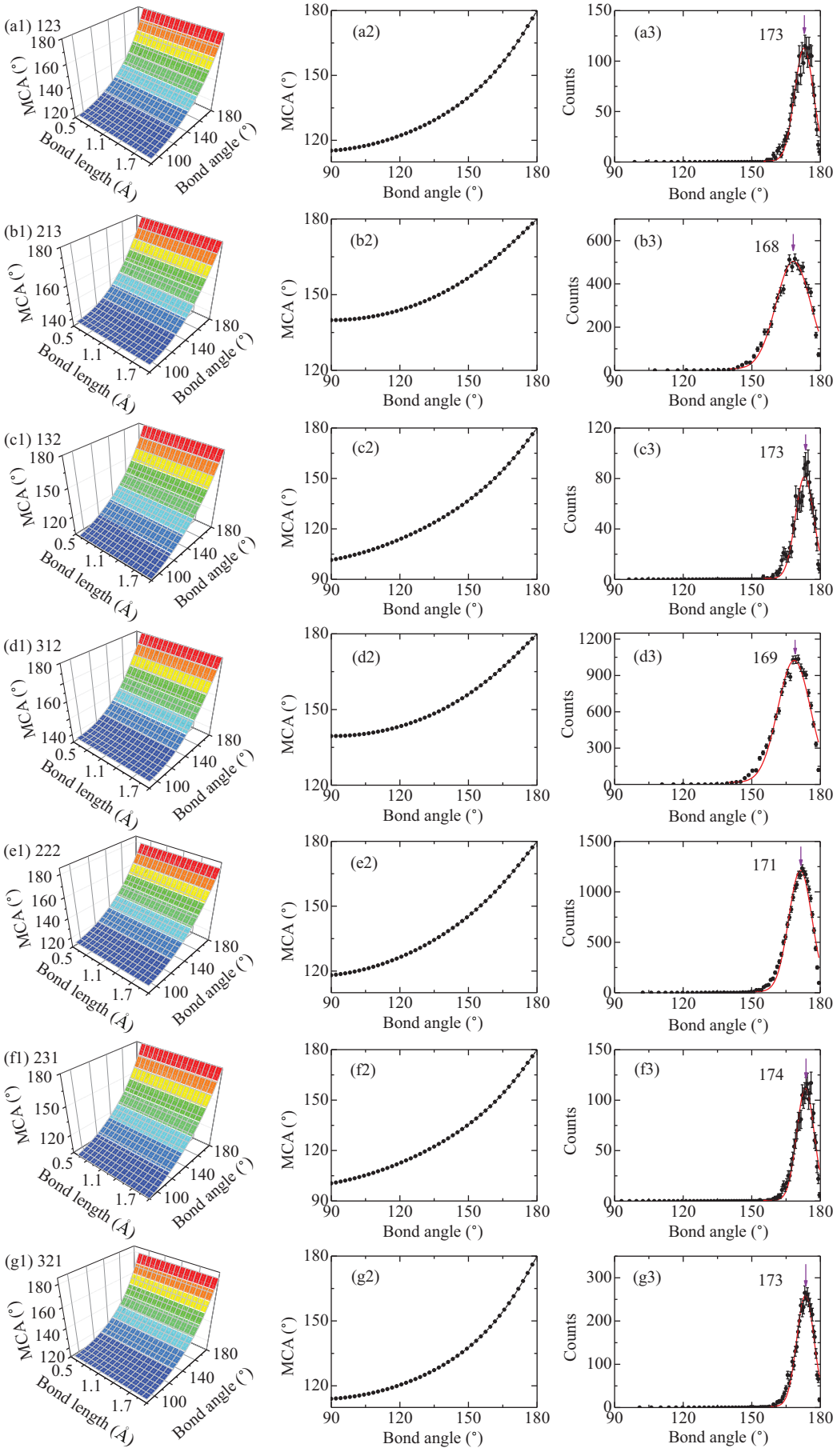


Fig. 4. The same as that of Fig. 3, but for the seven CE channels of N_2O^{6+}.

Not like diatomic molecules or symmetric triatomic molecules, for which only one bond length variable involved can be reconstructed conveniently according to the measured KER of the fragments in the CE model,[14,15] but for the asymmetric N_2O molecule, two variables of the N–N and N–O bond lengths make the reconstruction complex. In this work, a numerical computation is carried out to deduce the N–N and N–O bond lengths by solving the classical mechanical equations of motion for the three fragment ions of N_2O^{5+} and N_2O^{6+} explosion. In the calculation, it is assumed that the initial momenta of the respective atomic ions are zero, and only Coulombic force acts among the three fragment ions. For each of the CE channels, the bond angle is fixed by using the experimental most probable value while the N–N and N–O bond lengths vary separately with the step of 0.01 Å. Two variables are adjusted in a trial-and-error manner so that the calculated KER values for the terminal nitrogen, oxygen, and the sum of three ions simultaneously approach the corresponding experimental most probable values with less than 2% difference. In this way, the N–N and N–O bond lengths can be determined and listed in Table 1. It can be seen that for the channels (122), (131), (221), (123), (132), (222), (231) and (321) the derived N–N and N–O bond lengths are overall agreed with those of N_2O ($R_{N-N} = 1.13$ Å, $R_{N-O} = 1.19$ Å[47]). For other channels, the results obviously deviate from those of N_2O since the experimental KER values cannot be well predicted by the CE model. Possible factors may lie in: (1) the assumption of point charges is too simple for this multi-electron system. The point-charge picture implies that the nuclear charge of the fragment ions is 'fully' screened by the remaining electrons. At large distances this is usually a good approximation, while at the short distances in an exploding molecule the actual screening depends strongly on the occupation of individual orbitals. In this picture, an incomplete screening will finally result in larger kinetic energies observed. (2) The deformation of molecular geometry in the multi-ionization process results in a deviation from the equilibrium geometry of a neutral linear rigid molecule which is used in the CE model. (3) The fragment charges may be rearranged at a later stage of the dissociation process, which is different from the initial charge distributions generated in the ionization. For these possible factors, further experiments with the variable HCI or collision energies and theoretical calculations for the electronic states of highly charged molecular ions are expected.

4. Conclusion

The complete three-body Coulomb explosion of N_2O^{q+} ($q = 5, 6$) is studied in the collision of 56 keV/u Ne^{8+} projectile with N_2O gaseous target. Through the correlation analysis on the TOFs and the momentum conservation of three fragment ions, six CE channels for N_2O^{5+} and seven for N_2O^{6+} are identified. Using the measured KER and momentum correlation angles of the three ionic fragments for each of the CE channels, the N–N and N–O bond lengths and N–N–O bond angles of N_2O^{q+} prior to dissociation are determined by a numerical computation based on the CE model. For the channels (122), (131), (221), (123), (132), (222), (231) and (321), the mean values for the derived N–N and N–O bond lengths are 1.08 Å and 1.22 Å, respectively, consistent with those of neutral N_2O ($R_{N-N} = 1.13$ Å, $R_{N-O} = 1.19$ Å[47]). A tendency is found that when the charge of fragments from the central atom of a triatomic molecule is smaller than those of the terminal atoms, the fragmentation channel usually cannot be well described by the CE model. We suggest this kind of channels should be avoided for imaging molecular geometry by CEI technique. In general, the present study demonstrates the feasibility of the HCI-induced CEI and numerical computation methods to imaging molecular geometry, which will be a useful reference to the case of asymmetric polyatomic molecules.

References

[1] Vager Z, Kanter E P, Both G, Cooney P J, Faibis A, Koenig W, Zabransky B J and Zajfman D 1986 *Phys. Rev. Lett.* **57** 2793
[2] Vager Z, Naaman R and Kanter E P 1989 *Science* **244** 426
[3] Dörner R, Mergel V, Jagutzki O, Spielberger L, Ullrich J, Moshammer R and Schmidt-Böcking H 2000 *Phys. Rep.* **330** 95
[4] Ullrich J, Moshammer R, Dorn A, Dörner R, Schmidt L P H and Schmidt-Böcking H 2003 *Rep. Prog. Phys.* **66** 1463
[5] Baldit E, Saugout S and Cornaggia C 2005 *Phys. Rev. A* **71** 021403
[6] Wu C, Yang Y, Wu Z, Chen B, Dong H, Liu X, Deng Y, Liu H, Liu Y and Gong Q 2011 *Phys. Chem. Chem. Phys.* **13** 18398
[7] Legare F, Lee K F, Litvinyuk I V, Dooley P W, Bandrauk A D, Villeneuve D M and Corkum P B 2005 *Phys. Rev. A* **72** 052717
[8] Hishikawa A, Iwamae A, Hoshina K, Kono M and Yamanouchi K 1998 *Res. Chem. Intermed.* **24** 765
[9] Ueyama M, Hasegawa H, Hishikawa A and Yamanouchi K 2005 *J. Chem. Phys.* **123** 154305
[10] Karimi R, Bisson É, Wales B, Beaulieu S, Giguère M, Long Z J, Liu W K, Kieffer J C, Légaré F and Sanderson J 2013 *J. Chem. Phys.* **138** 204311
[11] Hishikawa A, Iwamae A and Yamanouchi K 1999 *Phys. Rev. Lett.* **83** 1127
[12] Bocharova I, Karimi R, Penka E F, Brichta J P, Lassonde P, Fu X, Kieffer J C, Bandrauk A D, Litvinyuk I, Sanderson J and Leǵare F 2011 *Phys. Rev. Lett.* **107** 063201
[13] Wu C, Wu C, Song D, Su H, Yang Y, Wu Z, Liu X, Liu H, Li M, Deng Y, Liu Y, Peng L Y, Jiang H and Gong Q 2013 *Phys. Rev. Lett.* **110** 103601
[14] Wu C, Wu C, Fan Y, Xie X, Wang P, Deng Y, Liu Y and Gong Q 2015 *J. Chem. Phys.* **142** 124303
[15] Wang E L, Shan X, Shen Z J, Li X Y, Gong M M, Tang Y G and Chen X J 2015 *Phys. Rev. A* **92** 062713
[16] Wang E L, Shan X, Shen Z J, Gong M M, Tang Y G, Pan Y, Lau K C and Chen X J 2015 *Phys. Rev. A* **91** 052711
[17] Siegmann B, Werner U, Lutz H O and Mann R 2002 *J. Phys. B: At. Mol. Opt. Phys.* **35** 3755
[18] Rajgara F A, Krishnamurthy M and Mathur D 2001 *Phys. Rev. A* **64** 032712
[19] Wang B, Han J, Zhu X L, Wei L, Ren B H, Zhang Y, Yu W D, Yan S C, Ma X W, Zou Y M, Chen L, and Wei B R 2021 *Phys. Rev. A* **103** 042810
[20] Pitzer M, Kunitski M, Johnson A S, Jahnke T, Sann H, Sturm F, Schmidt L Ph H, Schmidt-Böcking H, Dörner R, Stohner J, Kiedrowski J, Reggelin M, Marquardt S, Schieöer A, Berger R and Schöffler M S 2013 *Science* **341** 1096

[21] Herwig P, Zawatzky K, Grieser M, Heber O, Jordon-Thaden B, Krantz C, Novotny O, Repnow R, Schurig, Schwalm V D, Vager Z, Wolf A, Trapp O and Kreckel H 2013 *Science* **342** 1084

[22] Ulrich B, Vredenborg A, Malakzadeh A, Schmidt L Ph H, Havermeier T, Meckel M, Cole K, Smolarski M, Chang Z, Jahnke T and Dörner R 2011 *J. Phys. Chem. A* **115** 6936

[23] Wu J, Kuniski M, Schmidt L Ph H, Jahnke T and Dörner R 2012 *J. Chem. Phys.* **137** 104308

[24] Wu C, Wu C, Song D, Su H, Xie X, Li M, Deng Y, Liu Y and Gong Q 2014 *J. Chem. Phys.* **140** 141101

[25] Zhu X L, Yan S, Feng W T, Guo D L, Gao Y, Zhang R T, Zhang S F, Wang H B, Huang Z K, Zhang M, Hai B, Zhao D M, Wen W Q, Zhang P, Qian D B and Ma X 2017 *Nucl. Instr. Meth. B* **408** 42

[26] Chen L, Shan X, Zhao X, Zhu X L, Hu X Q, Wu Y, Feng W T, Guo D L, Zhang R T, Gao Y, Huang Z K, Wang J G, Ma X and Chen X J 2019 *Phys. Rev. A* **99** 012710

[27] Zhao X, Shan X, Zhu X L, Chen L, Shen Z J, Feng W T, Guo D L, Zhao D M, Zhang R T, Gao Y, Huang Z K, Zhang S F, Ma X and Chen X J 2021 *Phys. Rev. A* **103** 012802

[28] Wang D, Guo G, Min G and Zhang X 2017 *Phys. Rev. A* **95** 012705

[29] Werner U, Siegmann B and Mann R 2007 *Scientific Report 2006* (GSI Report 2007-1) p. 253

[30] Khan A, Tribedi L C and Misra D 2017 *Phys. Rev. A* **96** 012703

[31] Frasinski L J, Hatherly P A and Codling K 1991 *Phys. Lett. A* **156** 227

[32] Khan A and Misra D 2016 *J. Phys. B At. Mol. Opt. Phys.* **49** 055201

[33] Bhatt P, Singh R, Yadav N and Shanker R 2012 *Phys. Rev. A* **86** 052708

[34] Love N A and Price S D 2004 *Phys. Chem. Chem. Phys.* **6** 4558

[35] Eland J H D and Murphy V J 1991 *Rapid Commun. Mass Spectrom.* **5** 221

[36] Alagia M, Candori P, Falcinelli S, Lavollée M, Pirani F, Richter R, Strangesand S and Vecchiocattivi F 2006 *Chem. Phy. Lett.* **432** 398

[37] Price S D, Eland J H D, Fournier P G, Fournier J and Millie P 1988 *J. Chem. Phys.* **88** 1511

[38] Taylor S, Eland J H D and Hochlaf M 2006 *J. Chem. Phys.* **124** 204319

[39] Curtis D M and Eland J H D 1985 *Int. J. Mass Spectrom. Ion Process.* **63** 241

[40] Zhou X, Ranitovic P, Hogle C W, Eland J H D, Kapteyn H C and Murnane M M 2012 *Nat. Phys.* **8** 232

[41] Kübel M, Alnaser A S, Bergues B, Pischke T, Schmidt J, Deng Y, Jendrzejewski C, Ullrich J, Paulus G G, Azzeer A M, Kleineberg U, Moshammer R and Kling M F 2014 *New J. Phys.* **16** 065017

[42] Levasseur N and Millié P 1990 *J. Chem. Phys.* **92** 2974

[43] Zhang M, Najjari B, Hai B, Zhao D M, Lei J T, Dong D P, Zhang S F and Ma X W 2020 *Chin. Phys. B* **29** 063302

[44] Ma X, Zhu X, Liu H, Li B, Zhang S, Cao S, Feng W and Xu S 2008 *Sci. China Ser. G: Phys. Mech. Astron.* **51** 755

[45] Ma X, Zhang R T, Zhang S F, Zhu X L, Feng W T, Guo D L, Li B, Liu H P, Li C Y, Wang J G, Yan S C, Zhang P J and Wang Q 2011 *Phys. Rev. A* **83** 052707

[46] Wiley W C and McLaren I H 1955 *Rev. Sci. Instrum.* **26** 1150

[47] Harmony M D, Laurie V W, Kuczkowski R L, Schwendeman R H, Ramsay D A, Lovas F J, Lafferty W J and Maki A G 1979 *J. Phys. Chem. Ref. Data* **8** 619